ChemComm

Aggregation-induced circularly polarized phosphorescence of Pt(II) complexes with an axially chiral BINOL ligand

Journal:	*ChemComm*
Manuscript ID	CC-COM-11-2022-006198.R2
Article Type:	Communication

COMMUNICATION

Aggregation-induced circularly polarized phosphorescence of Pt(II) complexes with an axially chiral BINOL ligand

FReceived 00th January 20xx,
Accepted 00th January 20xx

DOI: 10.1039/x0xx00000x

Daiki Tauchi[a], Taiki Koida[a], Yuki Nojima[b], Masahi Hasegawa[b], Yasuhiro Mazaki[b], Akiko Inagaki[c], Ken-ichi Sugiura[d], Yuki Nagaya[e], Kazunori Tsubaki[e], Takuya Shiga[f], Yuuya Nagata[g], Hiroyuki Nishikawa[a]*

A pair of chiral Pt(II) complexes coordinated by simple BINOL and bipyridine ligands displaying aggregation-induced phosphorescence and circularly polarized luminescence were characterized by X-ray crystallography and absorption and emission spectroscopies. The emission of the powder sample was reddish whereas the thin film dispersed in PMMA (f_{Pf} = 1 wt%) exhibited a white emission.

The development of circularly polarized organic light-emitting diodes (CP-OLEDs) is of growing interest owing to their vast applications in advanced technologies, such as display technology, optical information communication, and chemical- and bio-sensing.[1] The application of several chiral luminescent compounds, ranging from small organic molecules to liquid crystals and polymers, as circularly polarized luminescence (CPL) emitters of CP-OLED has been reported.[2] Recently, chiral materials exhibiting thermally activated delayed fluorescence have been developed to successfully fabricate CP-OLEDs with a significantly high external quantum efficiency (EQE).[3] However, their electroluminescence dissymmetry factors (g_{EL}) are still unacceptable. On the other hand, organic nanostructures, such as chiral supramolecular structures of small molecules and π-conjugated polymers, and chiral liquid crystals generally exhibit a high luminescent dissymmetry factor (g_{CPL}).[4] Chiral arrangements of luminescent materials in the nanostructure aggregates impart the high g_{CPL} values. Therefore, the chiral materials with aggregation-induced emission (AIE) properties have great application potential as CPL emitters in CP-OLEDs with high g_{EL}. Chiral phosphorescent transition metal complexes composed of Ir(III)[5] and Pt(II)[6] ions have also been reported to exhibit circularly polarized electroluminescence (CPEL) with a relatively high EQE. Particularly, square planar Pt(II) complexes with chiral ligands have been extensively studied because of their circularly polarized phosphorescence.[7] In addition, supramolecular assemblies through noncovalent metal-metal and π-π interaction[8] or liquid crystalline states[6b, 9] usually exhibit high dissymmetry factors. However, there are only a few reports on the aggregation-induced phosphorescence (AIP)-active Pt(II) complexes with chiroptical properties even though the AIP-active chiral materials are good candidates for CP-OLEDs with high EQE.[6c, 10] Herein, a pair of chiral square planar tetradentate Pt(II) complexes, (*R*)-and (*S*)-[Pt(II)(BINOL)(bpy)] (***R*/*S*-Pt**, Fig. 1), was synthesized using commercially available ligands, 1,1'-binaphthalene-2,2'-diol (BINOL) and 2,2'-bipyridine (bpy). X-ray crystal structure analyses revealed that each enantiomer formed a 1-dimensional (1D) helical stacking structure by noncovalent π-π interaction between the ligands. The AIP properties were confirmed by the photophysical measurements both in solution and in solid-state. The chiroptical properties were evaluated through circular dichroism (CD) and CPL measurements. We performed density functional theory (DFT) calculations to understand the observed photophysical properties.

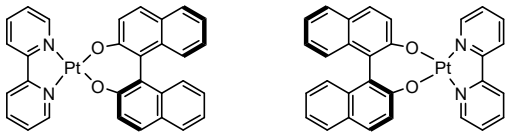

(*R*)-[Pt(II)(BINOL)(bpy)] (***R*-Pt**) (*S*)-[Pt(II)(BINOL)(bpy)] (***S*-Pt**)

Fig. 1 Molecular structure of (*S*)- and (*R*)-[Pt(II)(BINOL)(bpy)]

The chiral Pt(II) complexes, ***R*/*S*-Pt** were prepared from the Pt(II) bipyridine complex, [Pt(II)(bpy)Cl_2] and (*R*)- or (*S*)-BINOL in the presence of K_2CO_3 in 34% yield according to Scheme S1 in the Supporting Information.

X-ray crystallographic analyses of ***R*/*S*-Pt** were performed at 100 K for the block single crystals recrystallized from $CHCl_3$.

[a]*Graduate School of Science and Engineering, Ibaraki University, 2-1-1 Bunkyo, Mito, Ibaraki 310-8512, Japan. E-mail: hiroyuki.nishikawa.sci@vc.ibaraki.ac.jp*
[b]*Graduate School of Science, Kitasato University, Kanagawa 252-0373, Japan.*
[c]*Faculty of Science and Technology, Seikei University, Tokyo, 180-8633, Japan.*
[d]*Graduate School of Science, Tokyo Metropolitan University, Tokyo, 192-0397 Japan.*
[e]*Graduate School of Life and Environment Science, Kyoto Prefecture University, Kyoto 606-8522, Japan.*
[f]*Faculty of Pure and Applied Sciences, University of Tsukuba, Tsukuba 305-8577, Japan.*
[g]*Institute for Chemical Reaction Design and Discovery (WPI-ICReDD), Hokkaido University, Sapporo, Hokkaido 001-0021, Japan.*

†Electronic Supplementary Information (ESI) available: Experimental methods, preparation of the complexes, crystallographic data, spectroscopic data and results of theoretical calculation. CCDC 2213938 for *R*-Pt and 2213940 for *S*-Pt. For ESI and crystallographic data in CIF see DOI: 10.1039/x0xx00000x

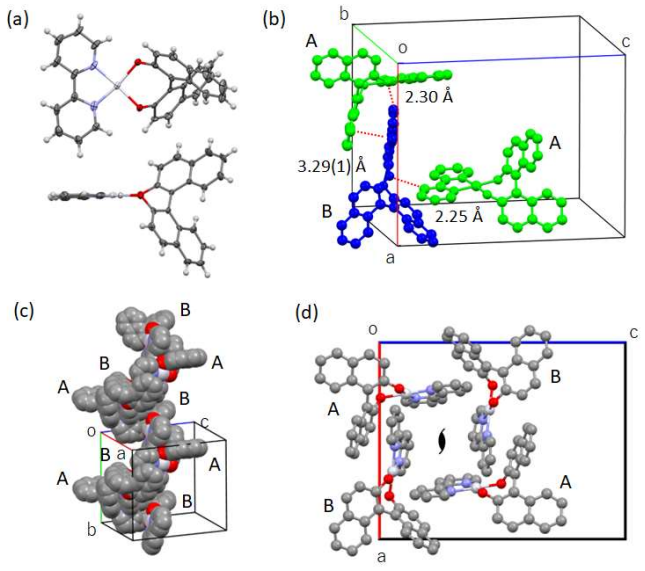

Fig. 2 Crystal structure of (*R*)-[Pt(II)(BINOL) (bpy)] (***R*-Pt**). (a) molecular structure; (b) Intermolecular interactions; (c) Helical assembly of ***R*-Pt**; (e) 1D helical column projected along b-axis. H atoms are omitted in (b), (c), and (d) for clarity.

Crystallographic data are listed in Table S1. Both enantiomers crystallized in the orthorhombic non-centrosymmetric space group $P2_12_12_1$ with two independent molecules (A and B) in the unit cell (Fig. 2(b)). The molecular and crystal structures of both the enantiomers mirrored each other (Fig. S7). As shown in Fig. 2(a), the Pt(II) ion in ***R*-Pt** adopts a slightly distorted square planar geometry (bond angles of A: 93.4(2)° (O-Pt-O), 81.5(3)° (N-Pt-N); bond angles of B: 93.0(3)° (O-Pt-O), 81.2(3)° (N-Pt-N)). The coordination bond lengths of the Pt(II) ions are in the range of 1.976(8)–2.002(7) Å for Pt-N and 2.003(7)–2.011(6) Å for Pt-O, which are typical of the Pt(II) bipyridine and binaphthyl complexes.[10a, 11] The dihedral angles between the two naphthyl groups of ***R*-Pt** are almost 72°, which are almost similar to those for Pt(II) complexes chelated by nitrogen atoms of BINAM (1,1'-binaphthalene-2,2'-diamine).[10a] The intermolecular π-π interaction (the shortest intermolecular C···C distance: 3.29(1) Å) exists between the naphthyl group of the molecule A and the bipyridyl group of the molecule B (Fig. 2(b)). There are also intermolecular interactions through C-H···O (2.25 and 2.30 Å) contact. These intermolecular interactions can arrange ***R*-Pt** to form a 1-dimensional (1-D) helix-like molecular arrangement with the *P*-helicity around the 2-fold screw axis along the b-axis (Fig. 2(c) and (d)). The ***S*-Pt** forms a 1-D helical array with the *M*-helicity (Fig. S7). Many C-H···π and C-H···O interactions are observed between the adjacent 1-D helical arrays, resulting in their interdigitation. Such strong intermolecular interactions within and between the 1-D helical structures, namely the 3-dimensional network structure, can restrict intramolecular motions, thereby inducing the AIP properties.

The UV-vis absorption spectra of ***R*/*S*-Pt** were recorded from the degassed and dilute CH_3CN solutions (1.0 x 10^{-5} M). The UV-vis absorption spectrum of ***R*-Pt** was calculated using the time-dependent density functional theory (TD-DFT) method at the level of CAM-B3LYP/Def2SVP. The calculated spectrum shifted by −0.29 eV to compensate overestimation of the vertical excitation eneryg by the CAM-B3LYP functional was found to be in good agreement with the observed spectrum (Fig. 3).[12] The selected TD-DFT calculated excitation energies, weights of main transitions, and related molecular orbitals (MOs), corresponding to the experimental absorption wavelengths are summarised in Table S3 and Fig. S22. The absorption band with a peak at 240 nm can mainly be assigned to the ligand-centered π-π* (BINOL) transitions and the shoulder band at 280 nm to a mixture of the ligand-centered π-π* (BINOL) and π-π* (bpy). The low-energy absorption bands observed at approximately 360 nm are mainly attributed to the singlet ^{1}MMLL'CT (Pt(5d) /BINOL→ bpy) transitions, similar to those observed for the square planar Pt dithiolene complexes.[7i, 13] The dominant transition at the absorption edge (~440 nm) is associated with the transition from the highest occupied MO (HOMO) to the lowest unoccupied MO (LUMO) (Table S3).

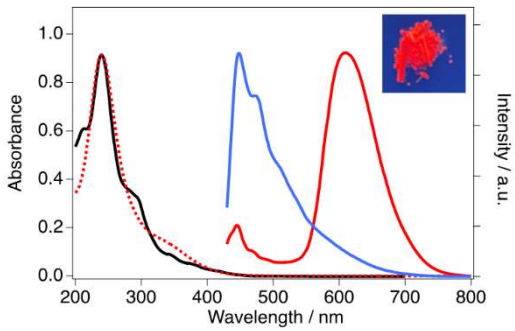

Fig. 3 The observed UV-vis absorption spectrum (black line, 1.0 x 10^{-5} M in CH_3CN) with the calculated spectrum (red dotted line) and photograph of the powder (inset), and the emission spectra in powder excited at 400 nm (red) and PMMA film (f_{Pt} = 1 wt%) excited at 380 nm(blue) of ***R*-Pt**.

The emissions of ***R*/*S*-Pt** were not observed in dilute CH_3CN, CH_2Cl_2, toluene, and THF solutions at a concentration of 1.0 x 10^{-5} M (Fig. S14). However, the powder sample and thin film dispersed in linear low-density poly(methyl methacrylate) (PMMA) exhibited phosphorescent properties, indicating an AIE character of these complexes (Fig. 3). The AIE properties were also confirmed by the emission measurements on the aggregates in THF-water mixed solvents. As shown in Fig. S11, when the fraction of water was higher than 80 %, the emission bands appeared in the range of 550–750 nm, similar to that of the powder sample. Dynamic light scattering analysis revealed the size distribution of aggregates formed in THF-water solution (fraction of water f_w = 95%) with a maximum intensity at *ca*. 100 nm (Fig. S15). The powder sample exhibited a broad range of emissions with a maximum value of 610 nm, and the emission of the powder sample was reddish (Fig. 3, inset). In contrast, the PMMA films cast from $CHCl_3$ solution (fraction of ***R*-Pt**: f_{Pt} = 1 wt%, thickness:

187 μm) exhibited a much broader emission with a vibronic band-like character ranging from the UV region to 750 nm (Fig. 3), resulting in a white emission (Fig. 4(a)). The Commission Internationale de L'eclairage (CIE) coordinates were x = 0.3106 and y = 0.3669. The photoluminescence quantum yields (PLQY) of the Pt complexes were 0.46 (***R*-Pt**) and 0.55 % (***S*-Pt**) for the powder and 0.085 (***R*-Pt**) and 0.14 % (***S*-Pt**) for the PMMA film states.

Such a low quantum yield is usually reported in the Pt complexes with non-cyclometalated ligands[7e, 7i, 10a]. The photoluminescence (PL) decay curve of the powder sample could be fitted by a double exponential function (Fig. S16), and the lifetime of the species with dominant decay was estimated to be 24 ns. On the other hand, fitting the decay curve of the PMMA film (f_{Pt} = 1 wt%) resulted in the existence of at least three components (Fig. S17): a faster component with a lifetime of 0.67 ns (52 %), one with a slightly faster lifetime of 8.3 ns (16 %) to the powder sample, and a slower one with a lifetime of 0.27 μs (33 %), indicating that the faster and slower components are associated with the aggregates of the Pt complex and the monomer, respectively. Thus, both the monomer and aggregate forms exist in the PMMA films (f_{Pt} = 1 wt%). We consider the emission at 600 nm exhibited by the powder to be attributed to the aggregates of the Pt complex, and the main emission centered at 450 nm from the PMMA film (f_{Pt} = 1 wt%) is attributed to monomer of the Pt complex. As shown in the emission spectrum of the PMMA film in Fig. 3, the intensity of the emission at 600 nm is rather small (shoulder), suggesting the amount of the aggregates is also very small in the PMMA film (f_{Pt} = 1 wt%). When the fraction of the Pt complex in the PMMA film increased from 1 wt% to 5 wt%, the intensity of the emission at 600 nm increased (Fig. S12), and the colors of the film changed from white (1 wt%) to orange (2 wt%) and red (5 wt%) (Fig. 4(a)). Consequently, the white emission from the PMMA film (f_{Pt} = 1 wt%) is associated with the mixture of the monomer and the aggregates of the Pt complex leading to the broad emission ranging from the UV region to 750 nm.

Chiroptical properties of ***R*/*S*-Pt** were investigated by CD and CPL spectra. The CPL spectra were acquired with excitations at 400 nm and 380 nm in the powders and PMMA films, respectively. Fig. 4(b) shows the CD spectra in dilute CH_3CN solutions (1.0 x 10^{-5} M) and the CPL spectra of powder samples. The CD signals of ***R*/*S*-Pt** exhibited mirror images with a molar circular dichroism ($\Delta\varepsilon$) of 60 M^{-1} cm^{-1} and dissymmetry factor $|g_{abs}|$ of 1.4 x 10^{-3} at 270 nm. The simulated CD spectra based on the TD-DFT calculation agreed with the experimental ones (Fig. S21), indicating the stereochemistries of ***R*/*S*-Pt** are retained in dilute CH_3CN solutions. The CPL signals of ***R*/*S*-Pt** in the powders appeared at 620 nm corresponding to their PL spectra. The g_{CPL} values at 621 nm of the ***R*-** and ***S*-Pt** are 3.4 x 10^{-3} and −2.3 x 10^{-3}, respectively, which are typical values of the Pt complexes previously reported[7a-c, 7g]. The ***R*/*S*-Pt** dispersed in PMMA films also exhibited CD and CPL spectra (Fig. S19). The wavelength regions of the CD and CPL signals corresponded to those of their absorption and PL spectra. The g_{CPL} values of the PMMA films at 459 nm were almost

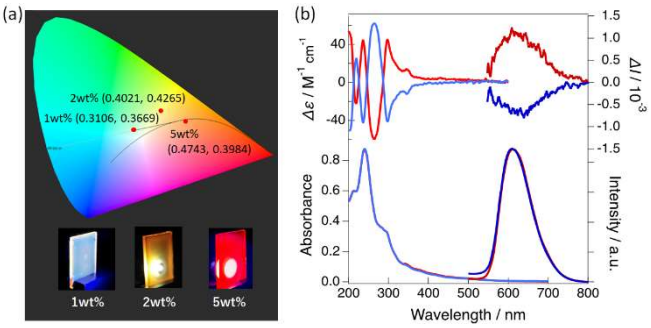

Fig. 4 (a) CIE coordinates of ***R*-Pt** dispersed in PMMA films of f_{Pt} = 1, 2, and 5 wt% with photographs of the PMMA films; (b) CD (upper left) and UV-vis (lower left) spectra in acetonitrile (1.0 x 10^{-5} M), and CPL (upper right) and PL (lower right) spectra in powder excited at 400 nm of ***R*-Pt** (red) and ***S*-Pt** (blue).

identical to those of the powders: 1.3 x 10^{-3} for the ***R*-Pt** and −2.4 x 10^{-3} for the ***S*-Pt**. Because the CD and CPL bands partially overlapped as shown in Fig. S19, the CPL could be caused by selected absorption of either right- or left-handed emission by the sample itself[14]. Further investigation should be needed to understand the origin of the CPL of the PMMA film. In addition, the aggregates in the THF-water mixed solution (f_w = 95%) showed a similar CPL signal to those of the powder sample (Fig. S20). Assuming the helical arrangement of ***R*/*S*-Pt** in the powders, PMMA films, and aggregates in the THF-water mixed solution, enhancement of dissymmetry factors could be expected by intermolecular excitonic coupling. But the g_{abs} values of the PMMA films (Table S2) were on the same order of 10^{-3} as those of the dilute CH_3CN solutions. Furthermore, the $|g_{CPL}|$ values of the powders and PMMA films (1.3–3.4 x 10^{-3}) are similar to those of similar Pt complexes in solutions previously reported.[7a, 7c] The comparison of the dissymmetry factors suggests that putative helical arrangements in the powders and PMMA films are unlikely to contribute to the chiroptical properties of this complex.

In conclusion, we developed novel AIP-active chiral Pt(II) complexes, ***R*/*S*-Pt**, using the commercially available simple ligands, BINOL and bpy. The X-ray single crystal structure analyses revealed that π-π and C-H···O interactions existed between adjacent complexes, resulting in the 1-D helical molecular arrangement. The AIP-activity of ***R*/*S*-Pt** was confirmed by the phosphorescence in the solid-state. ***R*/*S*-Pt** displayed red phosphorescence in the powder form whereas the thin films dispersed in PMMA exhibited white luminescence. Moreover, the complexes displayed both CD and CPL in the solid-state. White organic light-emitting diodes (WOLEDs) have also been gaining attention owing to their practical applications. While WOLEDs are typically fabricated by combining several materials that emit different colors, single-molecular WOLEDs have also been reported.[15] In contrast, only a few white light-emitting CP-OLEDs (CP-WOLEDs), which are based on the combination of CPL emitters[16] and mono-dispersed chiral polymers[17], have been reported. Although the

PLQYs of the complexes developed in this study were low, they exhibited white emission in the PMMA film. Therefore, this study can contribute to the development of novel single-molecular CP-WOLEDs based on CPL-active AIP emitters.

Acknowledgements

This work was supported in parts by MEXT KAKENHI (Grant No. JP18H01950), JSPS KAKENHI (Grant No. JP20K21167), JST CREST (Grant No. JPMJCR2001), and JST the establishment of university fellowship towards the creation of science and technology innovation (Grant No. JPMJFS2015).

Conflicts of interest

There are no conflicts to declare.

Notes and references

1. (a)Y. Imai, Y. Nakano, T. Kawai and J. Yuasa, *Angew Chem Int Ed Engl*, 2018, **57**, 8973-8978(b)D.-Y. Kim, *J Korean Chem Soc*, 2006, **49**, S505-S508(c)C. Li, X. Yang, J. Han, W. Sun and P. Duan, *Materials Advances*, 2021, **2**, 3851-3855(d)H. Li, H. Li, W. Wang, Y. Tao, S. Wang, Q. Yang, Y. Jiang, C. Zheng, W. Huang and R. Chen, *Angew Chem Int Ed Engl*, 2020, **59**, 4756-4762(e)N. Nishizawa, B. Al-Qadi and T. Kuchimaru, *J Biophotonics*, 2021, **14**, e202000380.
2. D. W. Zhang, M. Li and C. F. Chen, *Chem Soc Rev*, 2020, **49**, 1331-1343.
3. (a)Z. P. Yan, T. T. Liu, R. Wu, X. Liang, Z. Q. Li, L. Zhou, Y. X. Zheng and J. L. Zuo, *Adv Funct Mater*, 2021, **31**, 2103875(b)Y. Xu, Q. Wang, X. Cai, C. Li and Y. Wang, *Adv Mater*, 2021, **33**, e2100652(c)F. M. Xie, J. X. Zhou, X. Y. Zeng, Z. D. An, Y. Q. Li, D. X. Han, P. F. Duan, Z. G. Wu, Y. X. Zheng and J. X. Tang, *Advanced Optical Materials*, 2021, **9**, 2100017(d)L. Frédéric, A. Desmarchelier, L. Favereau and G. Pieters, *Adv Funct Mater*, 2021, **31**, 2010281.
4. (a)Y. Deng, M. Wang, Y. Zhuang, S. Liu, W. Huang and Q. Zhao, *Light Sci Appl*, 2021, **10**, 76(b)K. Akagi, *Bull Chem Soc Jpn*, 2019, **92**, 1509-1655.
5. (a)J.-J. Lu, Z.-L. Tu, X.-F. Luo, Y.-P. Zhang, Z.-Z. Qu, X. Liang, Z.-G. Wu and Y.-X. Zheng, *Journal of Materials Chemistry C*, 2021, **9**, 5244-5249(b)Z. P. Yan, K. Liao, H. B. Han, J. Su, Y. X. Zheng and J. L. Zuo, *Chem Commun (Camb)*, 2019, **55**, 8215-8218(c)T. Y. Li, Y. M. Jing, X. Liu, Y. Zhao, L. Shi, Z. Tang, Y. X. Zheng and J. L. Zuo, *Sci Rep*, 2015, **5**, 14912.
6. (a)Z. P. Yan, X. F. Luo, K. Liao, Y. X. Zheng and J. L. Zuo, *Front Chem*, 2020, **8**, 501(b)G. Qian, X. Yang, X. Wang, J. D. Herod, D. W. Bruce, S. Wang, W. Zhu, P. Duan and Y. Wang, *Advanced Optical Materials*, 2020, **8**, 2000775(c)Z. Jiang, J. Wang, T. Gao, J. Ma, Z. Liu and R. Chen, *ACS Appl Mater Interfaces*, 2020, **12**, 9520-9527(d)J. R. Brandt, X. Wang, Y. Yang, A. J. Campbell and M. J. Fuchter, *J Am Chem Soc*, 2016, **138**, 9743-9746(e)J. Song, H. Xiao, L. Fang, L. Qu, X. Zhou, Z. X. Xu, C. Yang and H. Xiang, *J Am Chem Soc*, 2022, **144**, 2233-2244(f)J. Han, Y. Wang, J. Wang, C. Wu, X. Zhang and X. Yin, *J Organomet Chem*, 2022, **973-974**.
7. (a)L. Yuan, Q.-J. Ding, Z.-L. Tu, X.-J. Liao, X.-F. Luo, Z.-P. Yan, Z.-G. Wu and Y.-X. Zheng, *Chin Chem Lett*, 2022, **33**, 1459-1462(b)M. Ikeshita, S. Furukawa, T. Ishikawa, K. Matsudaira, Y. Imai and T. Tsuno, *ChemistryOpen*, 2022, **11**, e202100277(c)P. Vazquez-Dominguez, O. Journaud, N. Vanthuyne, D. Jacquemin, L. Favereau, J. Crassous and A. Ros, *Dalton Trans*, 2021, **50**, 13220-13226(d)H. Zhu, Q. Li, B. Shi, H. Xing, Y. Sun, S. Lu, L. Shangguan, X. Li, F. Huang and P. J. Stang, *J Am Chem Soc*, 2020, **142**, 17340-17345(e)R. Inoue, R. Kondo and Y. Morisaki, *Chem Commun (Camb)*, 2020, **56**, 15438-15441(f)T. Usuki, H. Uchida, K. Omoto, Y. Yamanoi, A. Yamada, M. Iwamura, K. Nozaki and H. Nishihara, *J Org Chem*, 2019, **84**, 10749-10756(g)X. P. Zhang, L. L. Wang, X. W. Qi, D. S. Zhang, Q. Y. Yang, Z. F. Shi, Q. Lin and T. Wu, *Dalton Trans*, 2018, **47**, 10179-10186(h)T. R. Schulte, J. J. Holstein, L. Krause, R. Michel, D. Stalke, E. Sakuda, K. Umakoshi, G. Longhi, S. Abbate and G. H. Clever, *J Am Chem Soc*, 2017, **139**, 6863-6866(i)T. Biet, T. Cauchy, Q. Sun, J. Ding, A. Hauser, P. Oulevey, T. Burgi, D. Jacquemin, N. Vanthuyne, J. Crassous and N. Avarvari, *Chem Commun (Camb)*, 2017, **53**, 9210-9213(j)L. Norel, M. Rudolph, N. Vanthuyne, J. A. Williams, C. Lescop, C. Roussel, J. Autschbach, J. Crassous and R. Reau, *Angew Chem Int Ed Engl*, 2010, **49**, 99-102.
8. (a)B. Li, Y. Li, M. H. Chan and V. W. Yam, *J Am Chem Soc*, 2021, **143**, 21676-21684(b)Z.-L. Gong and Y.-W. Zhong, *Science China Chemistry*, 2021, **64**, 788-799(c)G. Park, H. Kim, H. Yang, K. R. Park, I. Song, J. H. Oh, C. Kim and Y. You, *Chem Sci*, 2019, **10**, 1294-1301(d)H. Sesolis, J. Dubarle-Offner, C. K. Chan, E. Puig, G. Gontard, P. Winter, A. L. Cooksy, V. W. Yam and H. Amouri, *Chemistry A European Journal*, 2016, **22**, 8032-8037(e)X. P. Zhang, V. Y. Chang, J. Liu, X. L. Yang, W. Huang, Y. Li, C. H. Li, G. Muller and X. Z. You, *Inorg Chem*, 2015, **54**, 143-152.
9. (a)B. Yang, G. Zou, S. Zhang, H. Ni, H. Wang, W. Xu, C. Yang, H. Zhang, W. Yu and K. Luo, *Angew Chem Int Ed Engl*, 2021, **60**, 10531-10536(b)B. Yang, H. Ni, H. Wang, Y. Hu, K. Luo and W. Yu, *The Journal of Physical Chemistry C*, 2020, **124**, 23879-23887.
10. (a)J. Song, M. Wang, X. Zhou and H. Xiang, *Chemistry A European Journal*, 2018, **24**, 7128-7132(b)T. Ikeda, M. Takayama, J. Kumar, T. Kawai and T. Haino, *Dalton Trans*, 2015, **44**, 13156-13162.
11. (a)J. Song, M. Wang, X. Xu, L. Qu, X. Zhou and H. Xiang, *Dalton Trans*, 2019, **48**, 4420-4428(b)F. Gou, J. Cheng, X. Zhang, G. Shen, X. Zhou and H. Xiang, *Eur J Inorg Chem*, 2016, **2016**, 4862-4866(c)*Acta Crystallogr Sect C: Cryst Struct Commun*, 1986, **C42**, 1701-1711.
12. C. Latouche, D. Skouteris, F. Palazzetti and V. Barone, *J Chem Theory Comput*, 2015, **11**, 3281-3289.
13. C. A. Mitsopoulou, *Coord Chem Rev*, 2010, **254**, 1448-1456.
14. E. Castiglioni, S. Abbate, F. Lebon and G. Longhi, *Chirality*, 2012, **24**, 725-730.
15. Z. Chen, C. L. Ho, L. Wang and W. Y. Wong, *Adv Mater*, 2020, **32**, e1903269.
16. (a)Y. P. Zhang, M. X. Mao, S. Q. Song, Y. Wang, Y. X. Zheng, J. L. Zuo and Y. Pan, *Angew Chem Int Ed Engl*, 2022, **61**, e202200290(b)Y. Zhang, J. Li, Y. Quan, S. Ye and Y. Cheng, *Chem. Eur. J.*, 2021, **27**, 589-593.
17. Y. Zhang, T. Jing, Y. Quan, S. Ye and Y. Cheng, *Advanced Optical Materials*, 2022, **10**, 2200915.